Journal of Energy Storage 83 (2024) 110767

Contents lists available at ScienceDirect

Journal of Energy Storage

journal homepage: www.elsevier.com/locate/est

Research papers

Design optimization of an innovative layered radial-flow high-temperature packed bed thermal energy storage

Silvia Trevisan *, Rafael Guedez

Department of Energy Technology, KTH Royal Institute of Technology, 100 44 Stockholm, Sweden

ARTICLE INFO

Keywords:
Thermal energy storage
Packed bed
Design multi-objective optimization
High temperature

ABSTRACT

The present work introduces an innovative layered radial flow packed-bed thermal energy storage able to provide enhanced thermal and hydrostatic performance, limiting their inherent trade-off. The performance of the proposed packed-bed thermal energy storage concept is modelled, in both thermal and hydrodynamic aspects, via a 1D-two phases numerical approach. Representative storage sizes for industrial applications and laboratory prototype are considered to highlight the potential for scaling and the representativeness of prototyping. Configurations with two and three coaxial layers are also analyzed. The investigation includes a multi-objective optimization of the thermal energy storage design considering a set of main design variables and a set of sensitivity analyses aimed at highlighting the influence of major operational parameters. The results show that the proposed storage geometry can provide simultaneous optimization of both thermal and hydrodynamic performance. The proposed storage unit could attain pressure drop reductions higher than 70 % with respect to uniform radial flow packed bed storage (and higher than 85 % with respect to axial flow units) at the expense of a useful duration reduction lower than 5 %. Industrial scale storage would benefit from low aspect ratios and arrangement with modular units, ensuring enhanced system flexibility and reduced parasitic consumptions thanks to lower pressure losses meanwhile guaranteeing extensive useful durations in both charge and discharge operation. Downscaled prototypes can provide a good representation of the thermal and hydrodynamic behavior of the proposed thermal energy storage solution and a relevant base for validation. This work paves the way for future prototyping and validation of the proposed layered radial flow packed-bed thermal energy storage concept.

1. Introduction

High-temperature thermal energy storage (TES) systems are becoming more and more relevant in the energy sector and they are recognized as key components in the future energy system [1]. High-temperature TES could enable waste heat recovery and facilitate the electrification of the hard-to-abate industrial sector by providing the needed flexibility [2,3]. The TES integration is also a key aspect of any concentrating solar power plant, ensuring dispatchable solar power and enabling lower levelized cost of electricity [4].

Packed bed TES (PBTES) systems store sensible thermal energy by heating and cooling solid particles by means of a heat transfer fluid (HTF) that flows through the bed. They have been shown to be an economically viable TES solution, particularly suitable for high temperature systems and applications [5]. Within the available literature, different packed bed TES designs have been proposed, investigated, and prototyped. Fig. 1 summarizes the most promising ones. The traditional cylindrical tank with axial HTF flow, sketched in Fig. 1(a), is the most mature solution and it has been deeply investigated both numerically [6,7], and experimentally [8–10]. Different solid materials (such as natural rocks [11], steel slags [12], and commercial ceramics as Al_2O_3 [13,14] or ZrO_2 [15]), working temperatures (with the largest operational range of 100 °C - 900 °C [16]), and HTFs (such as thermal oil [17], molten salts [18,19], air [9,20] and CO_2 [21]) have been considered. This PBTES design offers good thermal stability and limited thermocline degradation, leading to thermal efficiency higher than 90 % [7]. For liquid HTFs, inherently ensuring lower pressure drops, this design is shown to be the most relevant one for scaling up and industrial applications [22]. However, key drawbacks such as high sensitivity to thermal ratcheting and high thermomechanical load on the tank, as well as elevated thermal losses are still to be fully targeted. Additionally, when operated with gaseous HTFs this PBTES design causes elevated pressure drops, which results in high parasitic consumptions and elevated

* Corresponding author.
E-mail address: trevisan@kth.se (S. Trevisan).

https://doi.org/10.1016/j.est.2024.110767
Received 1 November 2023; Received in revised form 14 January 2024; Accepted 30 January 2024
Available online 3 February 2024

Nomenclature

Acronyms

AX	Axial flow
HTC	Heat transfer coefficient
HTF	Heat transfer flow
KPI	Key performance indicator
LR	Layer ratio
MOO	Multi-objective optimization
PBTES	Packed bed thermal energy storage
PCC	Pearson correlation coefficient
RAD	Radial flow
TES	Thermal energy storage

Symbols

c_p	Specific heat [J/(kg•K)]
D	TES diameter [m]
ΔT	Temperature difference [°C]
ΔTC	Thermocline thinckness
Δp_{TES}	Pressure drop [Pa]
Δr	Radial difference $\Delta r = r_{out}\text{-}r_{in}$ [m]
d_p	Particle diameter [mm]
E_{TES}	TES energy capacity [kWh]
G	Mass flow rate per unit area [kg/(m^2•s)]
H	TES height [m]
h	Convective heat transfer coefficient [W/(m^2•K)]
h*	Corrected convective heat transfer coefficient [W/(m^2•K)]
Nu	Nusselt's number
P	Power [kW]
Pr	Prandl's number
r	Radius [m]
$r_{A,B}$	Pearson correlation coefficient
Re	Reynold's number
t*	Useful duration [h]
T	Temperature [°C]
U_w	Overall heat transfer coefficient [W/(m^2•K)]
V	Volume [m^3]

Greek letters

α	Aspect ratio, $\alpha = \Delta r/H$
ε	Void fraction
η_0	Preliminary efficiency
μ	Mean
ρ	Density [kg/m^3]
σ	Standard deviation
τ*	Non-dimensional useful duration

Subscripts

ch	Charge
disch	Discharge
eff	Effective
F	Fluid
in	Inner
mid	Medium
out	Outer
S	Solid

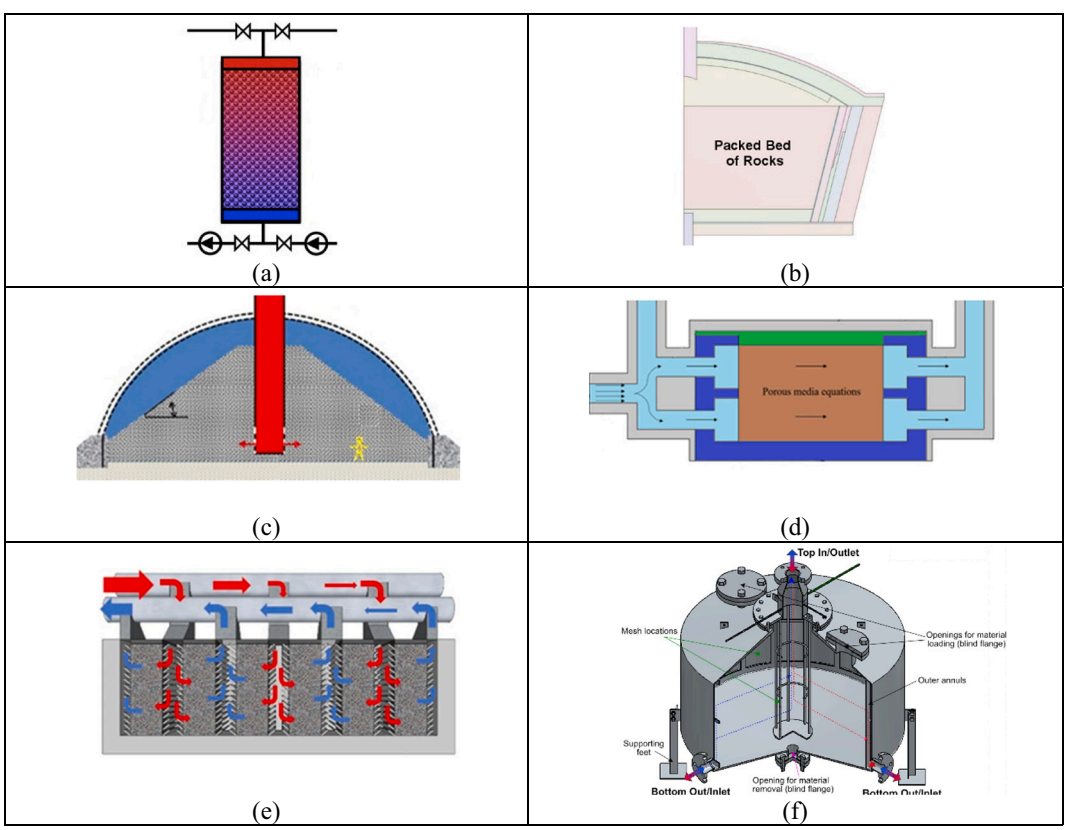

Fig. 1. Main packed bed TES designs investigated in the state of the art of the technology: (a) traditional cylindrical packed bed TES with axial HTF flow [8]; (b) buried truncated conical TES with axial HTF flow [23]; (c) self-insulated unconstrained packed bed TES [24]; (d) horizontal flow packed bed TES [25]; (e) modular layered packed bed TES with horizontal flow [26]; (f) radial-flow packed bed TES [27].

operational costs, which are likely to represent a major roadblock for upscaled industrial applications.

To address some of the challenges of traditional axial flow cylindrical PBTES some alternative designs have been proposed. *Zanganeh* et al. introduced a buried truncated conical TES with axial HTF flow, shown in Fig. 1(b) [23], later widely investigated for upscaled systems in [28]. The truncated conical shape limits the thermal ratcheting by guiding the particles upwards. However, the thermal losses from the top surface are increased due to the larger surface exposed to external airflow. The capital expenditure and the environmental footprint of the unit are increased due to the additional excavation cost and land impact. *Gauche* et al. introduced a self-insulated packed bed TES, made of an unconstrained pile of rocks packed around a central rigid pipe with a porous heat exchange region at the bottom, sketched in Fig. 1(c) [24]. This concept offers low installation costs and is self-insulated, reducing thermal losses and costs for insulation. However, it is also likely to lead to undesirable performance due to thermocline instabilities [29], linked to the unpredictability of the flow passage and distribution through the bed [30]. This would lead to operational issues and difficulties in attaining reliable system integration. A horizontal flow packed bed has been introduced in [25], shown in Fig. 1(d). The TES is similar to the traditional axial flow vertical tank, only differentiated by its orientation. Such an arrangement with dominant TES length over height would limit the ratcheting phenomenon and the thermomechanical load on the TES walls. However, particularly during standstill, buoyancy forces and natural convection would lead to temperature non-uniformities and vertical stratification causing lower thermal efficiency [31]. A PBTES concept characterized by modular parallel packed bed layers with horizontal flow has been developed by *Schlipf* et al., Fig. 1(e) [26]. The shorter length of each module can limit the issues highlighted before for horizontal PBTES arrangements. The modular design enables the utilization of different materials in each layer, increasing the TES flexibility. However, flow uneven distributions both along the vertical axis in each module and among the different modules have been measured [32].

A radial-flow packed bed TES design, shown in Fig. 1(f), has been proposed and tested by the authors [27] and numerically investigated also in [33]. This PBTES concept could offer self-insulation, leading to lowered thermal losses and limiting thermal ratcheting thanks to reduced temperature variability at the TES walls. The experimental validation of the unit confirmed limited pressure drops and thermal losses [27]. However, the temperature degradation and thermocline spread have been identified as the key drawbacks of this TES configuration limiting its efficiency to about 70 % for long operation cycles, while efficiencies higher than 90 % were obtained in a similar TES unit for shorter cycles [34].

Notwithstanding the relevant R&D work shown in literature, packed bed TES are not yet commercial solutions. Structural challenges, such as thermal ratcheting, thermal performance limitations, such as thermocline degradation, and operational requirements, such as elevated pressure drops, are the main limiting factors for packed bed commercialization. To boost the industrial application of packed bed TES these challenges should be addressed simultaneously, limiting the inherent trade-offs. The present work, builds upon authors' previous experiences [35], and aims at targeting the aforementioned challenges. Specifically, the work introduces an innovative layered radial flow packed-bed TES concept able to maintain the self-insulating arrangement and its consequential benefits, and to further reduce the pressure drop while improving the local heat transfer between fluid and solid maximizing the TES thermal performance. The performance of the TES concept is analyzed via a numerical investigation including multi-objective optimization and a wide range of sensitivity analyses. The results show that the proposed innovative packed bed TES design could ensure a large reduction of the pressure drop, leading to limited auxiliary power consumption, whilst improving the thermal performance of the unit. This work paves the way for the prototyping and validation of the proposed TES design.

2. Materials and methods

2.1. Innovative thermal energy storage concept description

A conceptual 2D axis-symmetric sketch of the innovative layered radial flow packed bed TES is shown in Fig. 2. The PBTES is comprised of multiple annular coaxial packed bed segments (shown and exemplified as S1, S2, and S3), a porous inner pipe and an outer annulus. During charge, the HTF enters from the inner central pipe, flows radially outwards crossing the layers from S1 to S3, is collected in the outer annulus, and exits from the lower outlet port. During discharge, the flow direction is reversed. The HTF enters from the outer annulus, travels the PBTES radially inward (from S3 to S1), is collected in the inner pipe and leaves the unit from the top outlet. As shown by the authors [35], in homogeneous single material radial flow packed bed TES, the HTF speed is higher in the inner region of the TES due to smaller cross-sectional area. A different HTF flow speed along the radial direction leads to an uneven development of the pressure drops and thermocline. The majority of the pressure losses occurs in the inner section, where higher flow speed is registered. Contrarily, the thermocline degradation is influenced by the effectiveness of the heat transfer between HTF and solids. The thermocline degrades more rapidly in the outer section of the TES, where the convective heat transfer is limited by the slower flow speed. From a TES design perspective, minimization of pressure drops and thermocline degradation typically requires contrasting approaches leading to critical trade-offs. The proposed PBTES design targets both performance metrics aiming at a comprehensive PBTES performance improvement. Specifically, in the inner layer (S1) an elevated heat transfer between HTF and solid is guaranteed by the high flow speed, while pressure losses should be reduced. Larger particles are introduced in S1 limiting the pressure drop. This will reduce the effective heat transfer area between HTF and solid material, however the elevated flow speed can counteract this decrease leading to limited reduction of the TES thermal efficiency. Contrarily, the outer section (S3) is filled with smaller particles which increase the heat transfer area between solid filler and HTF improving the convective heat transfer. Smaller particles will also hinder thermal radiation among particles, thus limiting the effective thermal

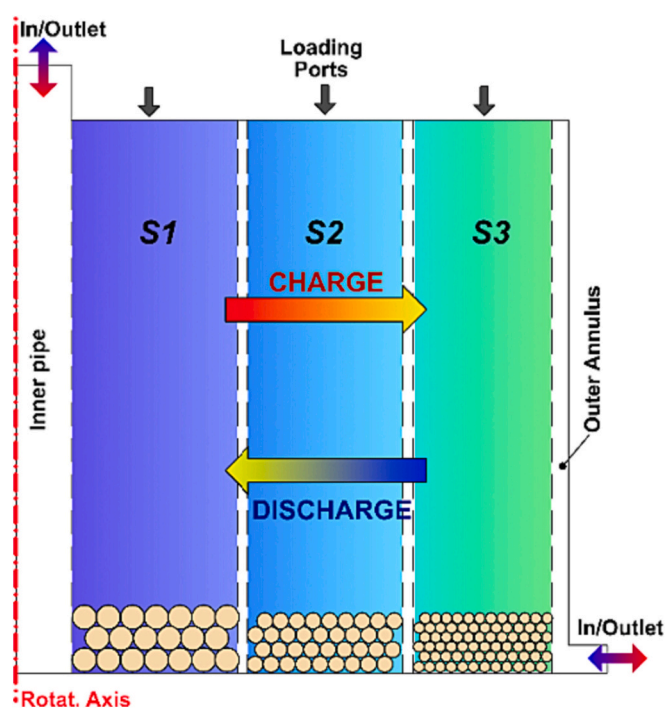

Fig. 2. 2D axis-symmetric sketch of the proposed innovative layered radial flow packed bed TES.

conductivity contributing to reducing the thermocline degradation. Thanks to the low flow speed in S3, the introduced smaller particles will not cause drastic increments of the pressure drop. Additionally, each layer has dedicated loading ports to facilitate the filling procedure and ensuring uniform void fractions. If required by the specific application, different materials could also be used in the different segments maximizing the TES flexibility.

2.2. Layered radial flow packed bed thermal energy storage modelling

In order to investigate the behavior of the proposed PBTES a preliminary sizing has been performed by considering the target TES energy capacity, E_{TES}, and Eq. (1).

$$V_{TES} = \frac{E_{TES}}{(\rho c_p)_{eff} \Delta T \eta_0} \tag{1}$$

Where, V_{TES} is the resulting volume of the PBTES, ΔT is the design temperature difference of the HTF equal to $T_{max} - T_{min}$, η_0 is the preliminary efficiency of the TES unit ensuring an oversizing of the TES unit account for thermal losses and thermocline degradation, $(\rho c_p)_{eff}$ is the effective energy density calculated as in Eq. (2).

$$(\rho c_p)_{eff} = \varepsilon \rho_F c_{p,F} + (1-\varepsilon)\rho_S c_{p,S} \tag{2}$$

Where, ε is the void fraction of the PBTES, ρ and c_p are the density and the specific heat of the solid or HTF, respectively. Air at ambient pressure (101.325 kPa) has been considered as the HTF and its thermodynamic properties have been gathered from the REFPROP database [36]. While commercial ceramics [37], with the properties listed in Table 1, have been considered as the solid filler material for the base PBTES configuration.

The HTF mass flow rate during charge and discharge, $\dot{m}_{ch/disch}$, has been assumed constant and equal between the two phases and evaluated as from Eq. (3).

$$\dot{m}_{ch/disch} = \frac{P_{ch/disch}}{c_{p,F} \Delta T} \tag{3}$$

Where, P is the target thermal power during operation. Two main TES energy capacities, E_{TES}, has been assessed: 10 MWh representative of an industrial installation also offering the opportunity for modularity, and a representative laboratory scale prototype of 50 kWh. Table 2 summarizes the main design parameters considered for the base configuration of both PBTES units.

The thermodynamic behavior of the PBTES has been described by adapting the Schumann model [38] to the radial geometry. Specifically, the 1D two phases model can be summarized by Eqs. (4) and (5), which describe the evolution of the fluid and solid temperature, respectively. This approach evaluates the temperature in 1D, considering uniform temperature distribution on the PBTES vertical direction. This assumption can be considered valid when limited standstill operation is considered, as in the case of this work which models consecutive charge and discharge phases. Vertical temperature distribution as well as natural convection phenomena would require more detailed 2-3D approaches.

Table 1
Properties of the considered solid filler materials as gathered from [37,46–48].

Material	Property		
	Density, ρ_S [kg/m^3]	Specific heat, $c_{p,S}$ [J/(kg•K)]	Thermal conductivity, k_S [W/(m•K)]
Commercial ceramic	2096.8	820	3
Steel slags	3500	950	1.5
Copper slags	3600	1300	1
Aluminum dross	2450	880	1

Table 2
Main PBTES design parameter for laboratory and industrial units.

Parameter	Value		Unit
	Industrial	Laboratory	
Energy capacity, E_{TES}	10,000	50	kWh
Minimum HTF temperature, T_{min}	200		°C
Maximum HTF temperature, T_{max}	800		°C
Preliminary efficiency, η_0	0.85		–
Void fraction, ε	0.38		–
Target power, $P_{ch/disch}$	4000	20	kW
Aspect ratio, $\alpha = \Delta r/H = (r_{out} - r_{in})/H$	1		–
Layer Ratio, LR - 2 coaxial layers	0.5		–
Layer Ratio 1, LR_1–3 coaxial layers	0.33		–
Layer Ratio 2, LR_2–3 coaxial layers	0.33		–
Inner layer particle diameter, $d_{p,in}$	80	20	mm
Mid layer particle diameter, $d_{p,mid}$	40	10	mm
Outer layer particle diameter, $d_{p,out}$	20	5	mm
Inner pipe diameter, D_{IN}	0.75	0.13	m

$$\frac{\partial T_F}{\partial t} + \frac{G}{\varepsilon \rho_F}\frac{\partial T_F}{\partial r} = \frac{k_{F,eff}}{\varepsilon \rho_F c_{p,F}}\left(\frac{1}{r}\frac{\partial}{\partial r}\left(r\frac{\partial T_F}{\partial r}\right)\right) + \frac{h a_s (T_S - T_F)}{\varepsilon \rho_F c_{p,F}} + \frac{U_w (T_\infty - T_F)}{H \varepsilon \rho_F c_{p,F}} \tag{4}$$

$$\frac{\partial T_S}{\partial t} = \frac{k_{S,eff}}{(1-\varepsilon)\rho_s c_{p,S}}\left(\frac{1}{r}\frac{\partial}{\partial r}\left(r\frac{\partial T_S}{\partial r}\right)\right) + \frac{h a_s}{(1-\varepsilon)\rho_s c_{p,S}}(T_F - T_S) \tag{5}$$

Where, G is the specific mass flow rate, H is the TES height, a_s is the shape factor, transposing h in the volumetric form, and defined as the packed bed surface to volume ratio equal to $6(1-\varepsilon)/d_p$, U_w is the heat transfer coefficient between the wall and the ambient air calculated as in [39], $k_{F,eff}$ and $k_{S,eff}$ are the effective thermal conductivities for the fluid and solid, respectively, they have been calculated following the procedures explained in [40,41], and h is the heat transfer coefficient between the solid filler material and the fluid flow, calculated by applying the Wakao's correlation as from Eq. (6) [42].

$$Nu = 2 + 1.1 \cdot Re^{0.6} \cdot Pr^{1/3} \tag{6}$$

Spherical particles, with sphericity equal to 1, have been assumed. In the case of a non-negligible thermal gradient within every single pebble (flagged by Biot's number higher than 0.1), caused by large particle diameter and low solid thermal conductivity, the HTC has been modified into h^*, which is defined in Eq. (7) [43] and has been extensively validated over a wide range of operating conditions and Re in an experimental work presented in [44].

$$\frac{1}{h^*} = \frac{1}{h} + \frac{d_p}{10 \cdot k_s} \tag{7}$$

To solve Eqs. (4) and (5), Dirichlet boundary conditions have been applied for the entering fluid equal to T_{max} during charge and T_{min} during discharge; Neumann boundary conditions with null heat flux have been considered at all other boundaries. Uniform temperature distribution has been assumed as the initial condition for both charge (equal to T_{min}) and discharge (equal to T_{max}).The pressure drop along the packed bed has been evaluated via the widely exploited Ergun's correlation, Eq. (8), [45]. It should be noted that this approach permits to account only for the pressure drop across the packed bed, not including the inner pipe and outer annulus of the TES unit. More detailed engineering should be performed to account for these additional pressure losses as well as other piping connections which might represent crucial losses in full scale system integrations.

$$\frac{\Delta p_{TES}}{(R_{out} - R_{in})} = 1.75\left(\frac{1-\varepsilon}{\varepsilon^3}\right)\frac{G^2}{\rho_F d_p} + 150\left(\frac{(1-\varepsilon)^2}{\varepsilon^3}\right)\frac{G \mu_F}{\rho_F d_p^2} \tag{8}$$

Validation of the above model, applied to axial geometry, has been

presented by the authors in [5], and supported for the radial geometry by the data presented by the authors in [35].

2.2.1. Storage multi-objective design optimization

In order to optimize comprehensively the thermodynamic and hydrodynamic performance of the proposed PBTES, a multi-objective optimization (MOO) approach has been followed. The model described in Section 2.2 has been applied to the PBTES geometries sketched in Fig. 3. The two geometries considered have two coaxial layers (Fig. 3(a)) and three coaxial layers (Fig. 3(b)). Both configurations have been analyzed and compared to identify the relevance and potential benefits offered by the introduction of additional layers. The main objective function considered in the PBTES design MOO is described by Eq. (9).

$$\overline{F} = min\left(\Delta p_{TES}, -t^{*}_{ch/disch}\right) \tag{9}$$

Where the two key performance indicators (KPI) considered are the pressure drop Δp_{TES}, as calculated in Eq. (8), and the useful duration of charge and discharge, $t^{*}_{ch/disch}$, defined as the time at which the outlet HTF temperature reaches the cut-off value. Due to the thermocline degradation during charge the HTF outlet temperature will remain around T_{min} for the initial part of the process, then it will start increasing. A charge cut off temperature equal to $T_{min} + 100\ °C$ has been imposed. Similarly, during discharge the HTF outlet temperature will remain around the maximum value in the beginning and then it will decrease. A discharge cut off temperature equal to $T_{max} - 100\ °C$ has been considered. Additionally, the maximum thermocline thickness reached during charge and discharge operation, $\Delta TC_{ch/disch}$, has been also calculated, as in Eq. (10) [39], and considered as a supportive performance indicator.

$$\Delta TC_{ch/disch} = \frac{\left| r|_{T_F = T_{max} - 50°C} - r|_{T_F = T_{min} + 50°C} \right|}{\Delta r} \tag{10}$$

Where, $\Delta r$is the radial distance traveled by the HTF equal to $r_{out} - r_{in}$. The useful duration of charge and discharge has been given more relevance during the optimization than the thermocline thickness since from an operational perspective this parameter has a higher influence over the TES, its system level integration and overall performance.

The influence of various design variables has been addressed in the MOO. In particular, particle diameter in the different layers, $d_{p,in}$, $d_{p,mid}$, and $d_{p,out}$, the relative thickness of the layers, defined as $LR = \left(r_{layer} - r_{in}\right)/\Delta r$, for the PBTES configuration with two coaxial layers and as $LR_1 = \left(r_{layer,1} - r_{in}\right)/\Delta r$ and $LR_2 = \left(r_{layer,2} - r_{layer,1}\right)/\Delta r$ for the PBTES configuration with three coaxial layers, and the aspect ratio, defined as $\alpha = \Delta r/H$, have been considered as decision variable during the PBTES design MOO. The considered ranges for the above listed decision variables are summarized in Table 3. Considering the high level of correlation between the above listed design variables, their individual influence over the TES KPIs has been quantified via the Pearson correlation coefficient (PCC), $r_{A,B}$, as defined in Eq. (11).

$$r_{A,B} = \frac{1}{N-1}\sum_{i=1}^{N}\left(\frac{A_i - \mu_A}{\sigma_A}\right)\left(\frac{B_i - \mu_B}{\sigma_B}\right) \tag{11}$$

Where, N is the number of observations (equivalent to the number of simulations run in the MOO, for all specific MOO the number of observations was always between 600 and 1200, thus ensuring validity and

Table 3
Values and constraints considered for the design decision variable in the TES design MOO. The main values listed refer tot the industrial scale TES unit (10MWh), while the values reported in the parathesis refer to laboratory scale TES (50kWh).

Variable	Minimum	Maximum	Step	Unit
Inner particle diameter, $d_{p,in}$	60 (12)	100 (22)	10 (2)	mm
Mid particle diameter, $d_{p,mid}$	20 (4)	60 (10)	10 (2)	mm
Outer particle diameter $d_{p,out}$	5 (2)	20 (8)	5 (2)	mm
Layer ratio, LR	0.1	0.9	0.1	–
Layer ratio 1, LR_1	0.1	0.7	0.1	–
Layer ratio 2, LR_2	0.1	0.7	0.1	–
Aspect ratio, $\alpha = \Delta r/H$	0.5	2	0.5 (0.25)	–

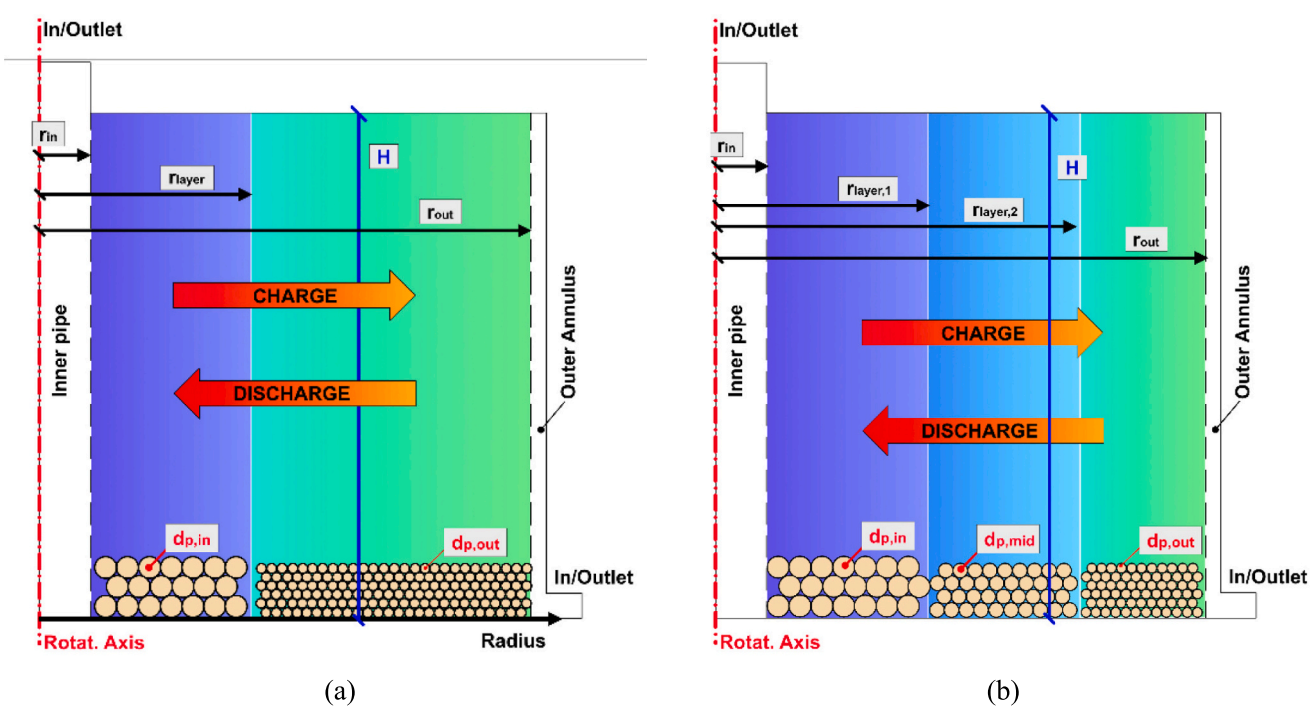

Fig. 3. 2D axis-symmetric representation of the considered PBTES geometry and main design variables for a PBTES unit with 2 coaxial layers (a) and a PBTES unit with 3 coaxial layers (b).

reliability for the evaluation of the PCC), and μ and σ are the mean and standard deviation of the variable and KPIs. To evaluate the correlation coefficients, all the simulations have been considered as the number of observations, not only the PBTES designs belonging to the Pareto fronts. It should be highlighted that the Pearson correlation coefficient can identify linear relationships among variables (a PCC equal to +1 implies a perfect positive relationship between variables; whilst a PCC equal to −1 implies a perfect negative relationship between variables), but it does not reflect parabolic (or higher order) type of relationships, thus possibly limiting the attainable insights.

The influence over the TES performance of operational variables such as the charge and discharge thermal power, and consequently the time duration of the TES, and the operating temperatures has been assessed via dedicated sensitivity analysis. Different solid filler materials, whose main thermodynamic properties are listed in Table 1 [37,46–48], have also been investigated. When changing operating conditions or solid filler materials the TES dimensions have been kept unchanged, so equal to the ones calculated for the base case using commercial ceramics operating between 200 °C and 800 °C.

3. Results and discussion

In this section, the main results are presented and discussed. Firstly, an overview of the main thermodynamic and hydrostatic behavior for a set of TES designs is shown. Secondly, the results of the proposed PBTES design MOO are presented for the industrial scale TES unit as well as the laboratory scale unit, aiming at highlighting the main different and representativeness of the downsized unit. Finally, the influence of some key operational parameters is shown via a set of sensitivity analysis.

3.1. General thermal and hydrodynamic behavior

Fig. 4 presents the HTF (solid lines) and solid (dashed lines) temperatures along the TES radial direction during charge (a) and discharge (b) at different time instants (after 10 min, 1 and 2 h) for three different PBTES arrangements with two coaxial layers and LR equal to 0.1, 0.5 and 0.9. The presented results refer to a laboratory sized TES unit, and similar temperature profiles are attained by the upscaled industrial TES. The inner layer, filled with larger particles, is highlighted by the grey area in Fig. 4. Similarly, Fig. 5 presents the HTF (solid lines) and solid (dashed lines) temperature along the TES radial direction during charge (a) and discharge (b) at different time instants (after 10 min, 1 and 2 h) for three different PBTES arrangements with three coaxial layers and different values of LR_1 and LR_2. The main sizing parameters of the TES units, including particle diameters, have been considered as for the base configuration listed in Table 2. The progressive flattening of the temperature curve during operation can be observed in all plots. The thermocline degradation is particularly relevant during discharge operation, during which flatter temperature curves can be observed leading to wider thermocline regions. The effect of particle size can be seen, for examples, by comparing the temperature behavior for a two coaxial layers PBTES configuration at LR = 0.1 and the one with LR = 0.9. Smaller particles grants larger heat transfer area between HTF and solid and higher heat transfer coefficients. This results in steeper temperature curves and thinner thermocline regions. This behavior can be observed also in the configurations with intermediate LR for which a change of the slope of the temperature curve in between two adjacent layers is visible. Additionally larger particle diameters also enlarge the temperature difference between the HTF and the solid due to a worsening of the heat transfer between HTF and solid. The introduction of a third additional coaxial layer, at least considering the specific particle sizes considered, does not affect largely the temperature profile with the PBTES units.

Fig. 6 highlights the hydrodynamic behavior and pressure drop reduction potential attainable by the proposed PBTES design with two coaxial layers, for both the industrial 10 MWh TES unit (Fig. 6(a)) and a 50 kWh prototype (Fig. 6(b)). The total pressure drop and its share between the inner and outer layer is shown for three different PBTES arrangements with LR equal to 0.1, 0.5 and 0.9. Inner particle diameter ($d_{p,in}$) of 80 mm and outer particle diameter ($d_{p,out}$) of 20 mm have been considered for the 10 MWh TES, while $d_{p,in}$ equal to 20 mm and $d_{p,out}$ equal to 5 mm have been applied to the 50 kWh unit. Similarly, the total pressure drop of two radial flow PBTES with uniform particle diameter of 20 mm and 80 mm (or 5 mm and 20 mm in the downsized TES) is shown (to enable a better understanding of the pressure drop distribution along the radius for these two examples with uniform particle size distribution the share between inner and outer layer assumes a LR equal to 0.5). To provide a better overview, the total pressure drop of two similarly sized axial flow PBTES with unitary aspect ratio, defined as $\alpha_{AX} = H/D$, and uniform particle diameter of 20 mm and 5 mm is also presented. Fig. 6 shows also the useful duration of charge and discharge operation for the different radial flow PBTES units considered. Firstly, it can be noted that the radial flow PBTES design ensure a pressure drop

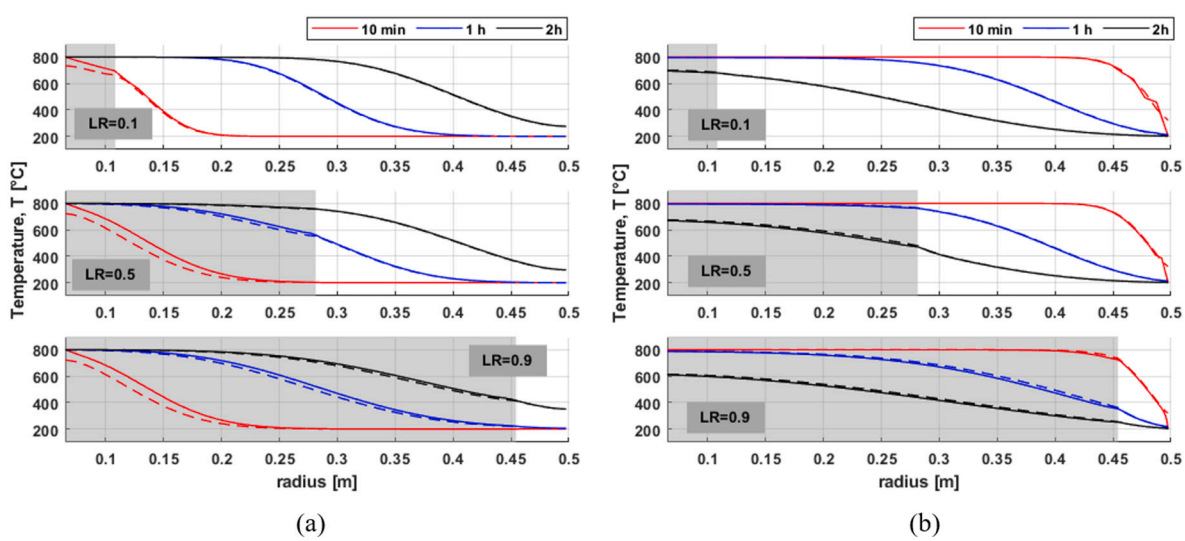

Fig. 4. (a) HTF (solid lines) and solid (dashed lines) temperature profile over the 2 coaxial layers PBTES radius for different LR during charge; (b) HTF (solid lines) and solid (dashed lines) temperature profile over the PBTES radius for different LR during discharge.

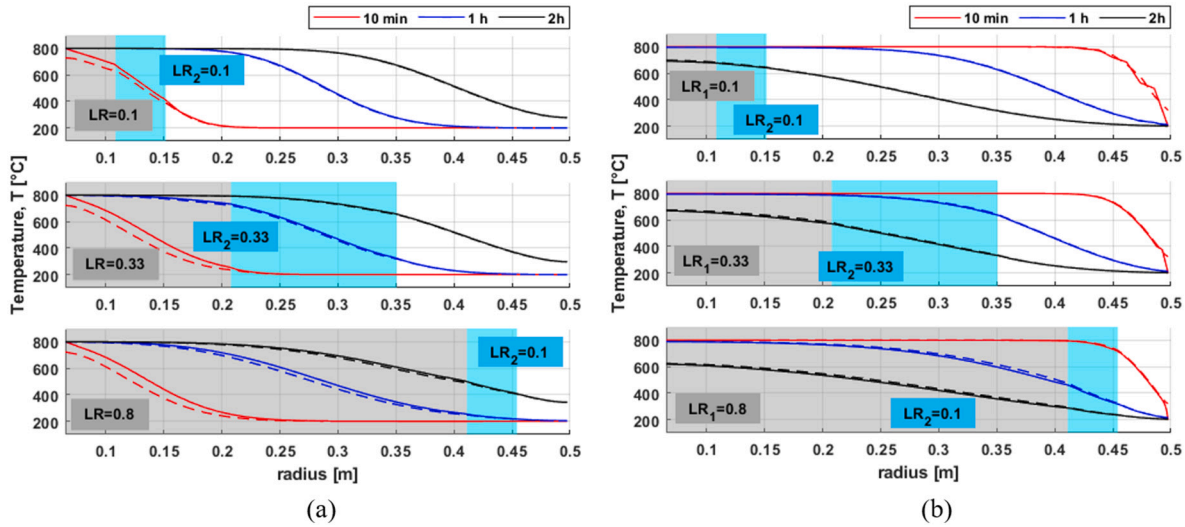

(a) (b)

Fig. 5. (a) HTF (solid lines) and solid (dashed lines) temperature profile over the 3 coaxial layers PBTES radius for different LR during charge; (b) HTF (solid lines) and solid (dashed lines) temperature profile over the PBTES radius for different LR during discharge.

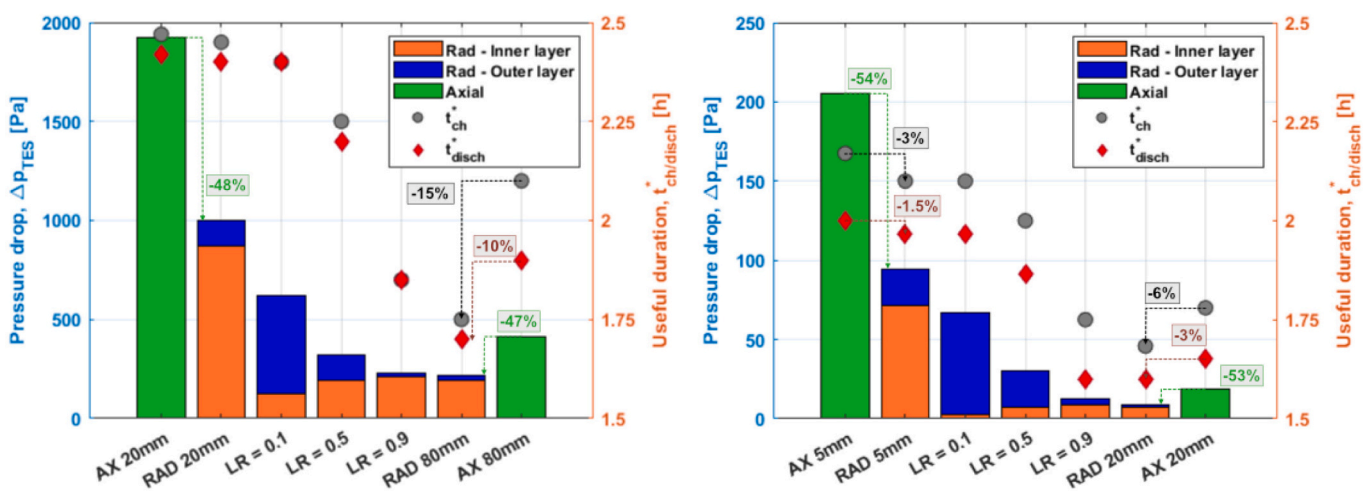

(a) (b)

Fig. 6. Pressure drop across the PBTES for the proposed design with 2 coaxial layer, considering different LR, and a similar reference PBTES with axial flow for a 10 MWh industrial unit (a) and a 50 kWh laboratory scale unit (b).

reduction of about 50 % with respect to similar axial flow PBTES units, both in the industrial and downsized unit. The radial TES lead to limited useful operation time reductions, generally below 6 % in lab scale units, and below 1 % for thermally effective large scale TES with small particles (i.e. AX 20 mm and RAD 20 mm). For larger particle size (i.e. RAD 80 mm) useful operation time reduction of about 15 % are recorded with respect to comparable axial flow PBTES. The layered design can attain further pressure drop reductions at the expenses of limited operation time reductions. In radial flow PBTES with uniform particle size more than 75 % of the total pressure drop occur in the innermost 50 % of the TES radius, as showed by the bars RAD 20 mm and RAD 80 mm (or RAD 5 mm and RAD 20 mm for the prototype unit). This highlights the need to act on the inner section of the TES unit to limit the parasitic losses. As an example, introducing larger particles (80 mm diameter against the original 20 mm) in the inner 50 % of the TES (LR = 0.5) leads to a total pressure drop reduction of about 68 % with respect to the homogenous 20 mm particle radial flow PBTES, and about 83 % with respect to the homogenous 20 mm particle axial flow PBTES. When looking at the influence of the LR a parabolic trend can be noted, with larger relative Δp_{TES} reductions attainable at small LR. A plateau can be reached for high LR, meaning that when most of the PBTES is already filled with large particles a further increment of LR does not produce a relevant hydrodynamic performance enhancement. The trade-off between thermal and hydrodynamic performance is evident when looking also at the useful duration of charge and discharge. PBTES units with reduced Δp_{TES} have lower $t^*_{ch/disch}$. However, introducing larger particles in the inner 50 % of the TES would cause a reduction of the useful operation time of only 8 % for large TES units and 5 % for prototype TES, whilst providing a pressure drop reduction of about 70 % with respect to a radial flow PBTES with uniform small particle diameter. This example highlights that beneficial results could be attained by the proposed TES unit largely reducing pressure drop at the expenses of limited reductions of the

useful operational time. The reported useful operation time also shows that the downscale TES units is more largely affected by inefficiencies and thermal losses. The $t^*_{ch/disch}$ for a 50 kWh TES unit is in average about 9 % lower than the one for a 10 MWh PBTES. Fig. 6 also indicates that for upscaled TES units the useful duration attained in charge and discharge are similar (with an average difference of 1.8 min), while an average difference of 7.4 min (equivalent to about 6 % of the average useful duration) is reported for a 50 kWh PBTES. This shows that the inefficiencies during the TES operation affect more relevantly the discharge phase and this is more visible in laboratory scaled TES units.

Similarly, Fig. 7 shows the pressure drop recorded for the proposed PBTES design with three coaxial layers, for a 10 MWh and a 50 kWh unit and considering a set of representative LR_1 and LR_2. The share of pressure drop in the different layers is also indicated together with the useful duration time both during charge and discharge. The wider the inner and intermediate layer the lower the total pressure drop. As visible also in Fig. 6, for larger TES units, the inner layers are responsible for a larger share of the total pressure drop. By comparing the PBTES with two or three coaxial layers, it can be observed that the differences of both total pressure drop and useful durations are limited. Thus, a PBTES with two coaxial layers could represent a better alternative thanks to its simpler construction.

3.2. Radial flow layered packed bed storage design optimization

Fig. 8 and Fig. 9 show the Pareto fronts obtained from the PBTES design MOO for a 10 MWh and a 50 kWh unit, respectively. The configurations with two coaxial layers are shown in Fig. 8(a) and Fig. 9(a) while the units with three coaxial layers are shown in Fig. 8(b) and Fig. 9 (b). The curves directly summarize the trade-off between pressure drop and useful duration of operation, during both charge and discharge. The color of the dots shows the maximum thermocline thickness measured during both operations. By comparing the plots, it can be observed that the addition of a third layer has a limited influence over the identified Pareto fronts and similar trends occur. This further confirms that layered PBTES with only two coaxial layers could serve the purposes whilst limiting construction challenges. In both TES sizes considered, the discharge phase suffers from wider thermocline spreads, due to the previously highlighted flatter temperature profiles in discharge operation. From Fig. 8, it can be observed that for an industrial sized PBTES an increase in the useful duration $t^*_{ch/disch}$ corresponds to thinner thermocline thicknesses ΔTC and charge and discharge operation phases are characterized by similar useful durations. The target useful duration of 2.5 h can be attained at a pressure drop lower than 500 Pa and at maximum thermocline thicknesses of about 0.3 during charge and o.55 during discharge. The long attained useful operation translate in a maximum thermal efficiency of the TES unit of about 88 %.

The laboratory scale PBTES unit is instead characterized by shorter useful operations, with a particular reduction for the discharge phase. This reduction translates also in a reduction of the TES thermal efficiency down to maximum values of about 76 % and 72 % in charge and discharge, respectively. In charge operation useful duration longer than 2 h are attained with thermocline thicknesses of about than 50 %. Contrarily, in discharge operation the ΔTC measured along the Pareto front is always higher than 70 %. PBTES configurations that cause high maximum thermocline spreads during discharge still ensure relatively high t^*_{disch} because in these units the thermocline spreads internally reaching the outlet at a late time. Thanks to this internal spread of the thermocline the outlet HTF temperature raises less rapidly ensuring sufficient t^*_{disch}. However, due to the poorer thermal performance achieved in discharge operation, in order to attain an useful duration of 2 h a PBTES units causing higher pressure drops, about twice the values measured during charge, is required.

3.2.1. Influence of design decision variables

Fig. 10 highlights the influence of the two most relevant design variables in the PBTES with two coaxial layers, the layer ratio LR (a-b) and the aspect ratio α (c-d), over the Pareto fronts for the 10 MWh and 50 kWh units. Their specific influence over the KPIs can be also observed, in the form of the Pearson correlation coefficient, in Fig. 11. Increasing the LR, meaning that larger sections of the PBTES are filled with bigger particles, causes reduced pressure drops but worse thermal performance. Lower pressure drops are ensured thanks to the lower HTF flow blockage effect of wider particles. Worse thermal performance is due to lower effective heat transfer areas and convective heat transfer coefficients in the regions with larger particles. A similar trend can be observed for both industrial and laboratory scaled PBTES. However, for laboratory scaled units a larger set of the Pareto front is characterized by LR higher than 0.5. This difference is related to the different selection of aspect ratio along the Pareto fronts for the industrial and lab scale PBTES. In large scale applications, the pressure drop becomes more relevant; thus, TES configuration with low α and Δp_{TES} are preferred. To

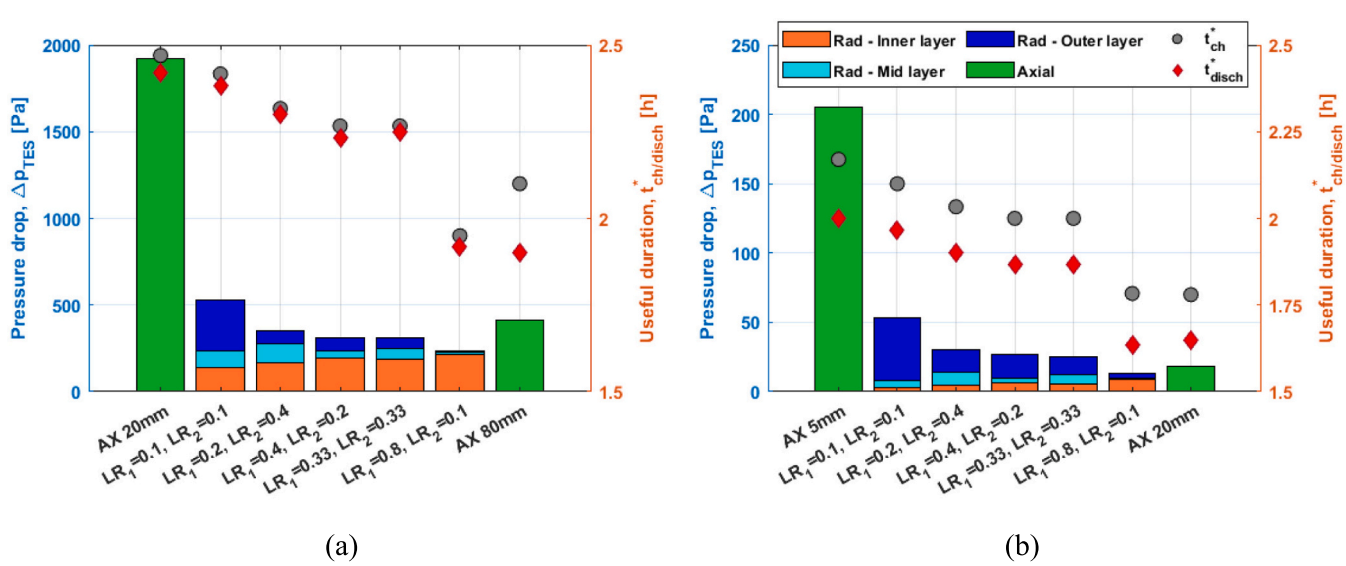

Fig. 7. Pressure drop across the PBTES for the proposed design with 3 coaxial layers for a 10 MWh industrial unit (a) and a 50 kWh laboratory scale unit (b) considering different representative LR_1 and LR_2.

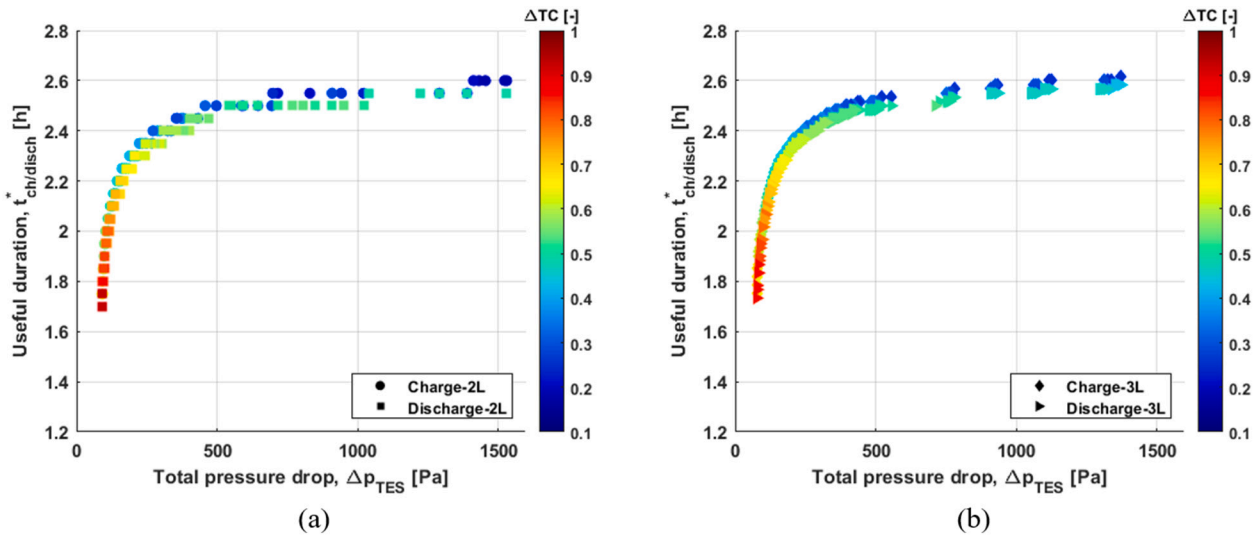

Fig. 8. Pareto fronts from the multi-objective optimization of the KPIs (pressure drop and useful time of charge and discharge) of the proposed PBTES design with 2 coaxial layers (a) and with 3 coaxial layers (b) (for an industrial 10 MWh PBTES unit), also showing the maximum thermocline thickness.

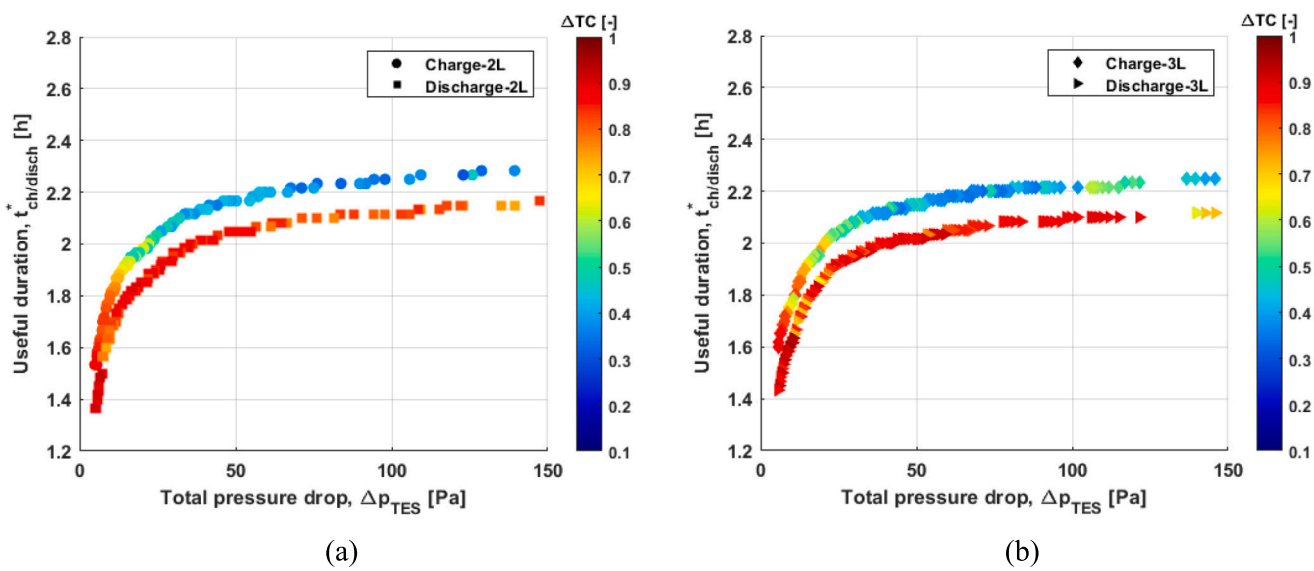

Fig. 9. Pareto fronts from the multi-objective optimization of the KPIs (pressure drop and useful time of charge and discharge) of the proposed PBTES design with 2 coaxial layers (a) and with 3 coaxial layers (b) (for a 50 kWh PBTES unit), also showing the maximum thermocline thickness.

achieve such pressure drop reduction, the most relevant design parameter to act upon in industrial scale units is the aspect ratio, as testified also by a $r_{\alpha,\Delta p_{TES}}$ of 0.7 (against a $r_{LR,\Delta p_{TES}}$ of −0.24). Contrarily, in laboratory scaled units the LR has the largest influence with a $r_{LR,\Delta p_{TES}}$ of −0.57, while $r_{\alpha,\Delta p_{TES}}$ is limited to 0.27. A high LR causes shorter useful duration both in charge and discharge, as testified by the negative r_{LR,t^*}. The worsening of the TES thermal performance caused by increasing LR, particularly in industrial units, is also highlighted by the increase of the thermocline thickness. High TES aspect ratios provide longer useful durations but at the expense of higher pressure drops. The influence of α over the TES thermal performance in laboratory scaled PBTES is relevant, as shown by r_{α,t^*} higher than 0.6, and compensate for the increased pressure drop. Contrarily, in industrial systems the thermal benefits provided by high aspect ratios are less relevant (r_{α,t^*} of about 0.24). Thus, on the Pareto front α is limited to up to 1. It should be remembered that low aspect ratios imply taller TES units which would suffer from higher stresses on the walls. This might represent a critical roadblock for further upscaling and massive radial flow PBTES installations, unless targeted via a modular approach.

Fig. 11 summarizes the Pearson correlation coefficients $r_{A,B}$ between the considered KPIs and design variables for a radial flow PBTES with two coaxial layers considering an industrial Fig. 11 (a) and a laboratory scale Fig. 11 (b) PBTES. The values for LR and α sustain the trends and explanations provided before. Additionally, it can be observed that the particle diameter has a less relevant influence over the KPIs than LR or α with r values between −0.06 and 0.06 in industrial sized PBTES and between −0.15 and 0.11 in lab scale units. As expected, an increase of the particle size limits the pressure drop but it also causes shorter useful durations. Considering the limited influence of the particle size, it is suggested to act of the LR and aspect ratio (while keeping larger particles in the inner layer and smaller ones in the outer section) to optimize the TES thermodynamic and hydrodynamic performance.

Fig. 12 presents the Pearson correlation coefficients between the considered KPIs and geometrical design variables for a radial flow PBTES with three coaxial layers. The TES aspect ratio has a clear

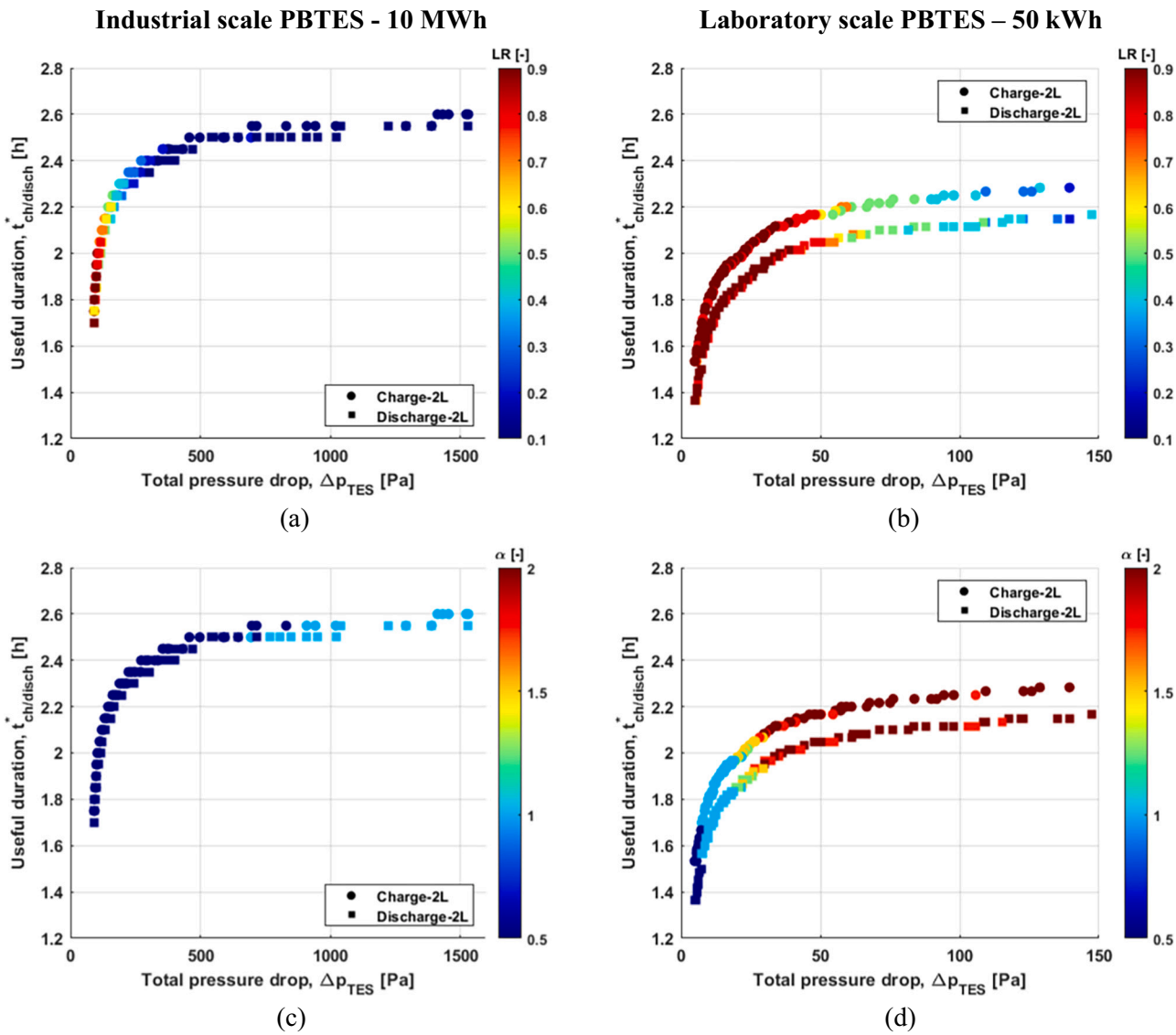

Fig. 10. Influence of the LR (a-b) and of the TES aspect ratio (c-d) over the identified Pareto curves for a 10MWh and a 50 kWh PBTES with 2 coaxial layers.

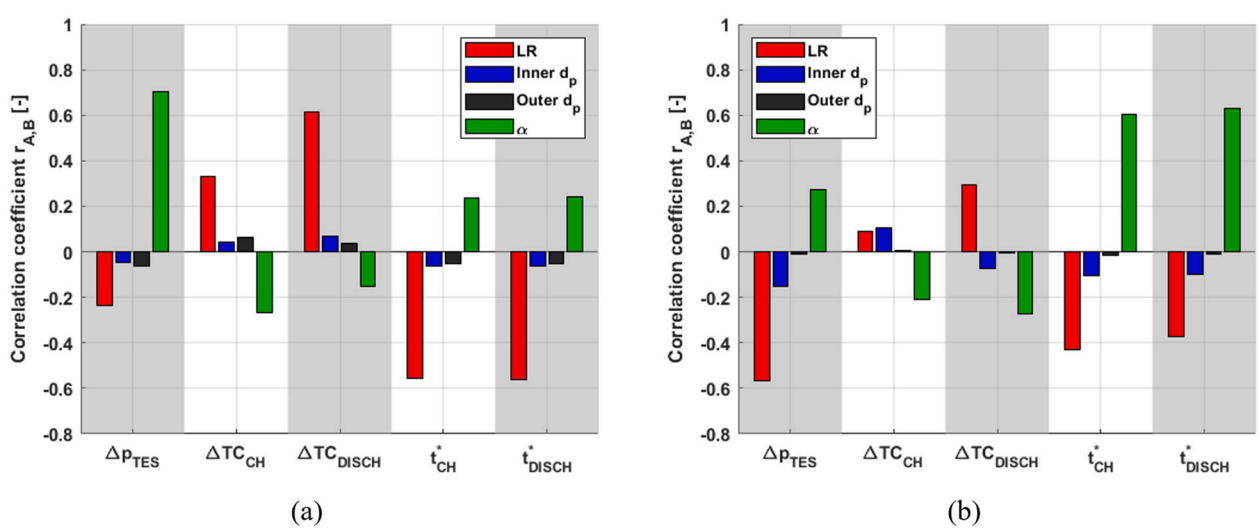

Fig. 11. Pearson correlation coefficients between the considered KPIs and geometrical design variables for a 10 MWh (a) and a 50 kWh (b) PBTES units with 2 coaxial layers.

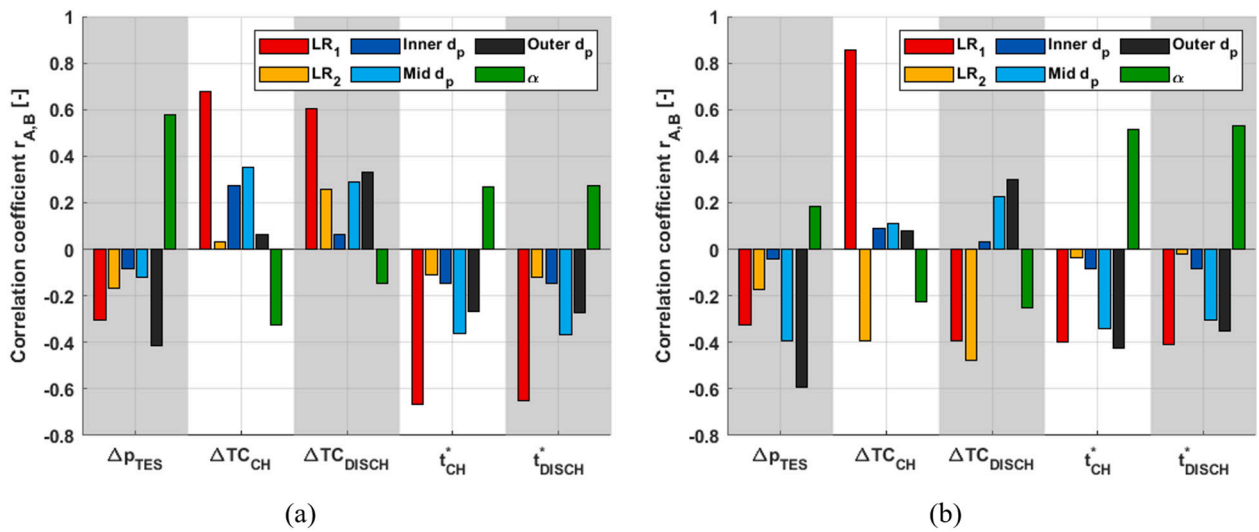

Fig. 12. Pearson correlation coefficients between the considered KPIs and geometrical design variables for a 10 MWh (a) and a 50 kWh (b) PBTES units with 3 coaxial layers.

influence over the performance of the TES and as highlighted before a different relevance depending on the size of the TES unit. For industrial scale PBTES low aspect ratios are preferred and still provide relevant thermal performance, again sustained by a $r_{\alpha,\Delta p_{TES}}$ of almost 0.6. Contrarily for laboratory scale units, higher aspect ratios are required to achieve longer useful operation though also causing higher pressure drops. Low α ensures limited pressure losses but has detrimental effect over the thermal performance of the TES unit, both trends supported by a $r_{\alpha,\Delta p_{TES}}$ of about 0.2 and r_{α,t^*} higher than 0.55. Increasing LR_1 provides reduced pressure drops but worse thermodynamic performance, particularly causing reductions of the useful duration in charge and discharge. Specifically, LR_1 around 0.2 and in the range 0.3–0.4 (coupled with α higher than 1) are suggested for industrial systems and laboratory one, respectively. LR_2 shows similar influences over the considered KPIs; however, its impact is in average less relevant than the inner LR. For laboratory scaled units, an increase of both LRs causes a reduction of the maximum thermocline thickness measured during discharge. This behavior is mostly due a reduced heat transfer between HTF and solid at larger particle causing a faster release of the thermocline and a faster decrease of the TES outlet temperature during discharge, as testified by negative $r_{LR,t^*_{disch}}$. In contrast with the PBTES configuration featuring two coaxial layers, in the unit with three layers the particle diameters have a more relevant impact over the TES performance. In particular, the outer particle size shows the highest Pearson correlation coefficients. Larger $d_{p,out}$ can widely contribute to reducing the pressure drop with $r_{d_{p,out},\Delta p_{TES}}$ as low as −0.4 and − 0.6 for industrial and prototype sized PBTES. However, an increase of $d_{p,out}$ has also non negligible effect on the PBTES thermal performance, as shown by $r_{d_{p,out},t^*}$ between −0.42 and − 0.25. In particular, industrial PBTES would require $d_{p,in}$ in the range 70–80 mm and $d_{p,out}$ of about 15 mm. Instead, optimal laboratory scale (50 kWh) PBTES units would present $d_{p,in}$ in the range 17–21 mm and $d_{p,out}$ in the range 6–7 mm. The specific influence of some of most relevant design variables over the Pareto fronts in the PBTES configuration is shown in the Appendix.

3.3. Assessment of main operational conditions

The influence of the target operation time over the PBTES performance is summarized by Fig. 13 (thermal KPIs) and Fig. 14 (Δp_{TES}) for both industrial and laboratory scale units with two coaxial layers. It

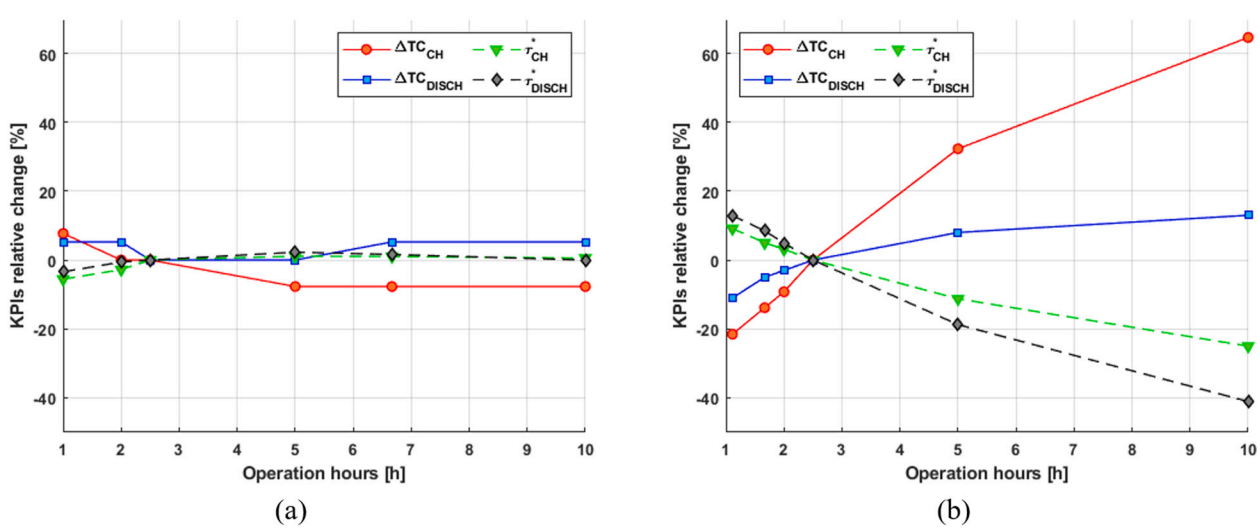

Fig. 13. Influence of the target time of operation (linked to the charge and discharge power) over the thermal KPIs for a PBTES of 10 MWh (a) and 50 kWh (b).

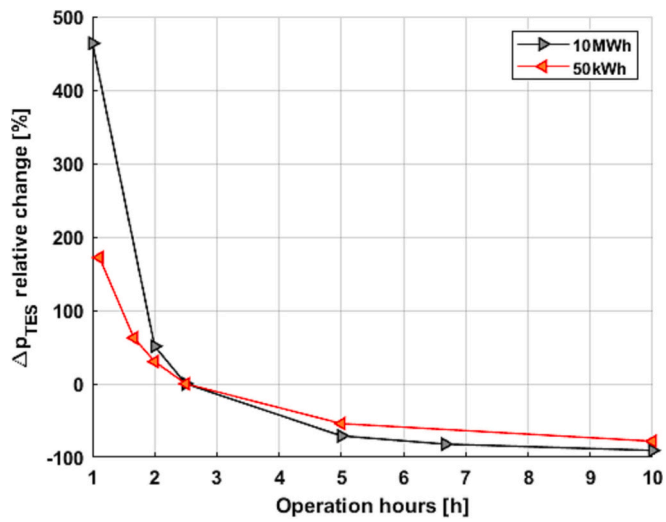

Fig. 14. Influence of the target time of operation (linked to the charge and discharge power) over the pressure drop for a PBTES of 10 MWh (a) and 50 kWh (b).

should be highlighted that in looking at different target operation time the TES energy capacity has been maintained constant (10 MWh and 50 kWh) while the power during charge and discharge has been modified accordingly to the target operation time. All the other design parameters describing the PBTES units have been maintained as from the base configurations summarized in Table 2. The results are reported as percentage changes with respect to the values observed in the base case TES configuration (characterized by a target operation time of 2.5 h). Since the differences between configurations with two and three coaxial layers are negligible, only the data for two co-axial layers are shown. Firstly, it can be noted that the operating power has higher influence over the pressure drop when considering industrial units and a much higher influence on the thermal performance when looking at laboratory scale TES. Such difference is due to the fact that pressure drop is a dominant KPI for industrial units, which are instead generally characterized by higher thermal performance. Pressure drop in industrial scale PBTES has a major influence due to larger flow rates, particularly at high power rates.

For industrial scale PBTES a change in the charge and discharge power will lead to relative changes of the thermal KPIs in the range ± 10 %. The best operating conditions can be identified for a target operation time of 5 h (equivalent to a power during charge and discharge of 2 MW), which can provide an increase of the useful operation time of up to 2 % and a reduction of the maximum thermocline thickness during charge of about 8 %. Such target operation time would also lead to a reduction of the pressure drop by about 70 %. These results suggest that modular approaches (with multiple TES units interconnected) for upscaled systems are likely to result in optimal operational performance. As previously noted, modular installations would not only limit the over pressure drop at the expenses of limited thermal performance reductions, but they would also ensure lowered mechanical and structural risks in upscaling, limiting the stresses on the TES walls.

For laboratory scale PBTES different target operating times might lead to thermal KPIs variations in the range − 40 % to +60 %. Higher power rates (resulting in shorter operating times) would lead to improved thermal performance with up to 12 % longer useful duration and thermocline thicknesses reduced by more than 10 % for a target operating time of 1 h. The improvement of the thermal performance is largely related to the lower thermal performance and higher influence of thermal losses typical for laboratory and small-scale installations. The thermocline thickness during charge is the KPI the most affected by the power rate, showing an increase of more than 60 % for very slow operation (i.e. target operating time of 10 h).

Fig. 15 and Fig. 16 show the influence of the maximum and minimum operating temperatures of the PBTES over the thermal KPIs for all PBTES configurations analyzed. Similar trends can be noted also between the industrial and laboratory scaled unit, showing full representativeness of laboratory prototypes on this point. The maximum operating temperature has a wider influence on the PBTES performance. Higher T_{max} causes an increase of the thermal losses toward the surrounding environment (even more relevant in small scale TES) and an increment of the effective thermal conductivity of the packed bed, leading to a more rapid spread of the thermocline region and a faster change of the HTF outlet temperature with consequent reduction of the useful duration. T_{max} has a negligible influence on the pressure drop due to limited relative changes of the HTF properties at high temperatures. The minimum operating temperature has a limited influence over the PBTES thermal performance, with KPIs relative changes in the range ± 10 %. A change of T_{min} shows a contrasting influence with respect to the

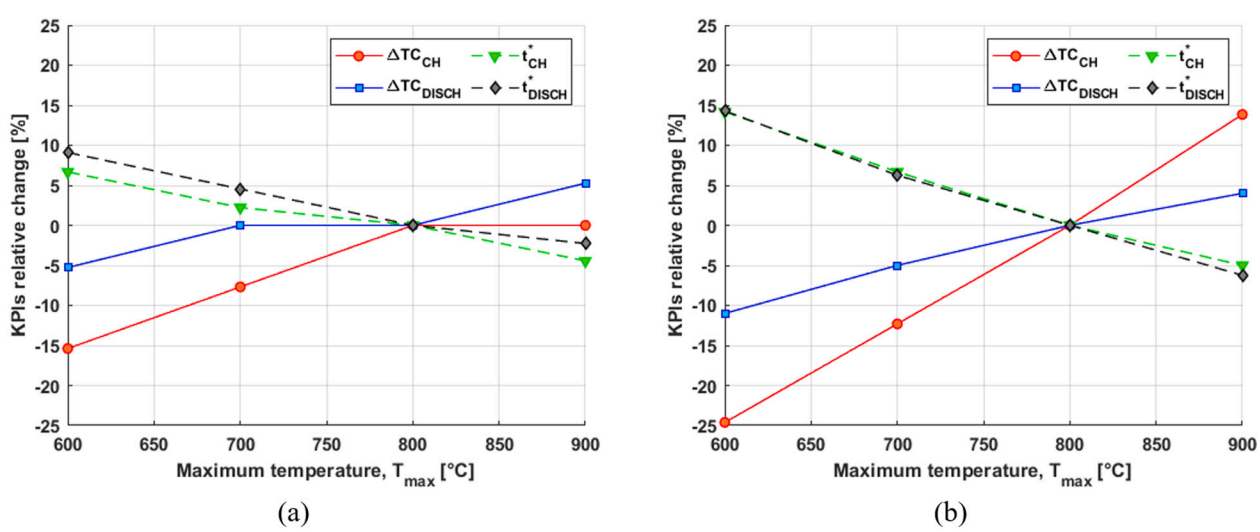

Fig. 15. Influence of the maximum operating temperature over the thermal KPIs for a PBTES of 10 MWh (a) and 50 kWh (b).

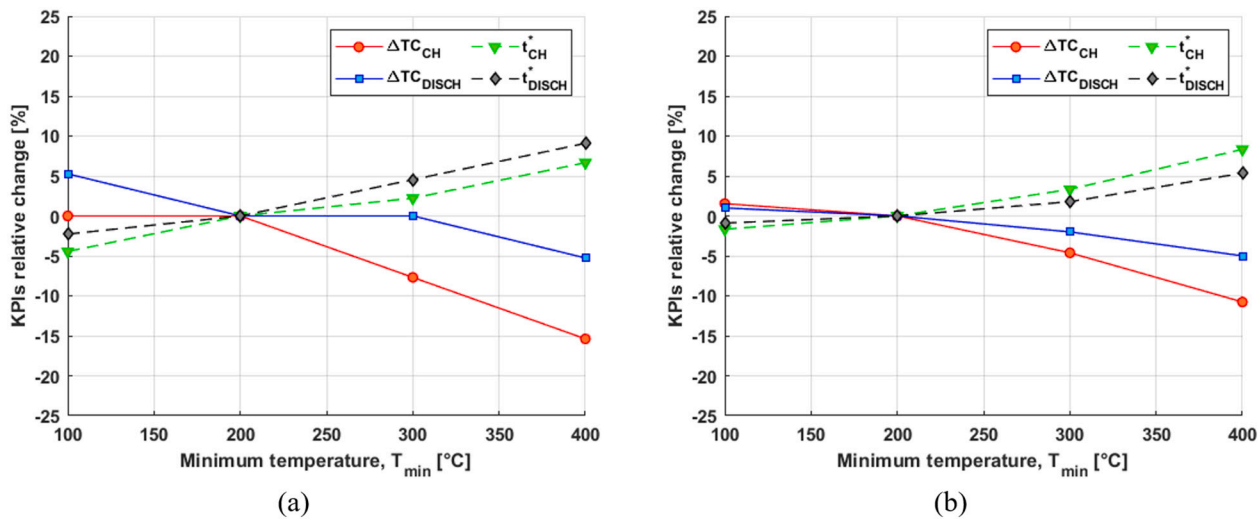

Fig. 16. Influence of the minimum operating temperature over the thermal KPIs for a PBTES of 10 MWh (a) and 50 kWh (b).

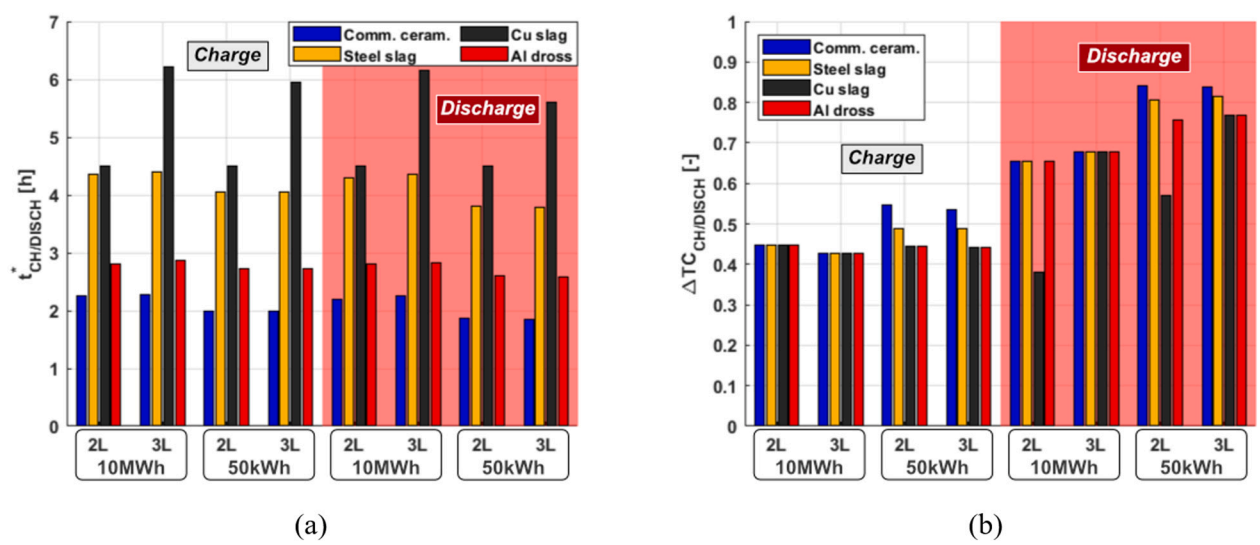

Fig. 17. Influence of the solid filler material over the useful duration in charge and discharge (a) and over the maximum thermocline thickness during charge and discharge (b) for all considered PBTES configurations.

described impact of T_{max}. This shows that, regardless of the specific working temperature, changes in the operating temperature difference ($T_{max} - T_{min}$) would have a similar impact on the PBTES thermal performance. Increasing T_{min} causes an increase of Δp_{TES} due to the increased viscosity and reduced density of the HTF. At higher T_{min}, and lower operating temperature differences for the PBTES, the thermal performance improves thanks to a reduced effect of thermal conduction, which contributes to reducing the thermocline spread.

Lastly, Fig. 17 summarizes the influence of the filler material over the TES thermal KPIs. Comparable outcomes are attained for industrial scale and prototype scale TES unit; thus, showing the potential for relevant laboratory testing and reliable upscaling. The material selection has a negligible influence on the hydrodynamic performance, considering that for all materials a unitary sphericity has been assumed, which might not always be achievable from a manufacturing perspective.

Instead, the filler material has a higher impact over the thermodynamic performance of the PBTES and particularly its useful duration during both charge and discharge. Materials with higher energy density, such as copper slags, permit to attain longer useful duration particularly for PBTES configurations with three coaxial layers. Materials with high thermal conductivity cause flatter temperature profiles over the TES radius. However, in large scale PBTES, the maximum thermocline thickness is not directly affected by the solid filler material since the variability of thermal conductivity showed by the considered materials is limited. In laboratory scale TES unit, the effect of the thermal conductivity is more visible, showing decreasing ΔTC for lower materials with lower thermal conductivity, such as copper slags and aluminum dross. Overall, copper slags seem to be a very promising PBTES material thanks to its elevated energy capacity and low thermal conductivity.

4. Conclusions

The present work has introduced an innovative layered radial flow packed-bed TES concept able to provide self-insulation while enhancing thermal and hydrostatic performance, limiting the inherent trade-off between them. The performance of the proposed packed-bed TES

concept has been analyzed based on a 1D-two phases thermal and hydrodynamic numerical model. Packed-bed TES configurations with two and three coaxial layers have been considered. Additionally, the study analyses the performance of an industrial size TES unit (10 MWh) and compares this against a laboratory size prototype (50 kWh) aiming at highlighting the potential for relevant TES downsizing and the scalability of laboratory testing campaign and results. The investigation includes a multi-objective optimization of the TES design considering a set of major design variables and a set of sensitivity analyses over the main operating parameters. From the presented results the following main conclusions can be drawn:

1. The introduced innovative layered radial-flow high-temperature packed bed thermal energy storage could enable comprehensive storage design optimization targeting simultaneously both thermal and hydrodynamic performance.
2. The presented innovative layered radial-flow high-temperature packed bed thermal energy storage could attain pressure drop reductions higher than 70 % with respect to uniform radial flow packed bed storage and higher than 85 % with respect to axial flow units at the expenses of a useful duration reduction lower than 5 %.
3. The addition of a third coaxial layer has only a minimal influence on the overall attainable thermodynamic and hydrostatic performance of the storage unit, suggesting that two coaxial layers would be sufficient whilst limiting the construction challenges.
4. The aspect ratio and the layer ratio are the most relevant design variables to be considered, showing contrasting influence over the accounted performance indicators.
5. Large scale layered radial-flow high-temperature packed bed thermal energy storage would benefit from low aspect ratios and arrangement with modular units. This would ensure enhanced system flexibility and reduced parasitic consumptions due to pressure losses meanwhile guaranteeing extensive useful durations in both charge and discharge operation. Overall, thermal efficiency as high as 88 % could be attained.
6. Downscaled prototypes of the proposed PBTES can provide good representation of the thermal and hydrodynamic performance of the solution and a relevant based for validation. When downsizing the proposed TES solution, main attention should be paid on the discharge operation which shows worse performance. Operation at different power rates can also lead to wider thermal performance variations.

This work paves the way for the prototyping and validation of the proposed layered radial flow packed-bed TES concept. Additionally, future works will be focused on the upscaling of the TES unit, addressing the highlighted challenges, and investigating modular solutions targeting solar thermal applications and the industrial heat decarbonization market.

CRediT authorship contribution statement

Silvia Trevisan: Writing – original draft, Visualization, Validation, Software, Resources, Methodology, Investigation, Funding acquisition, Formal analysis, Data curation, Conceptualization. **Rafael Guedez:** Writing – review & editing, Supervision, Project administration, Methodology, Funding acquisition, Conceptualization.

Declaration of competing interest

The authors declare that they have no known competing financial interests or personal relationships that could have appeared to influence the work reported in this paper.

Data availability

Data will be made available on request.

Acknowledgement

This project has received funding from the European Union's Horizon Europe research and innovation programme under grant agreement No 101083899.

Appendix A

Fig. A summarizes the influence of some of most relevant design variables over the Pareto fronts in the PBTES configuration with three coaxial layers for an energy capacity of 10 MWh and 50 kWh. Specifically, the aspect ratio α, the inner layer ratio LR_1 and the inner and outer particle diameter are shown.

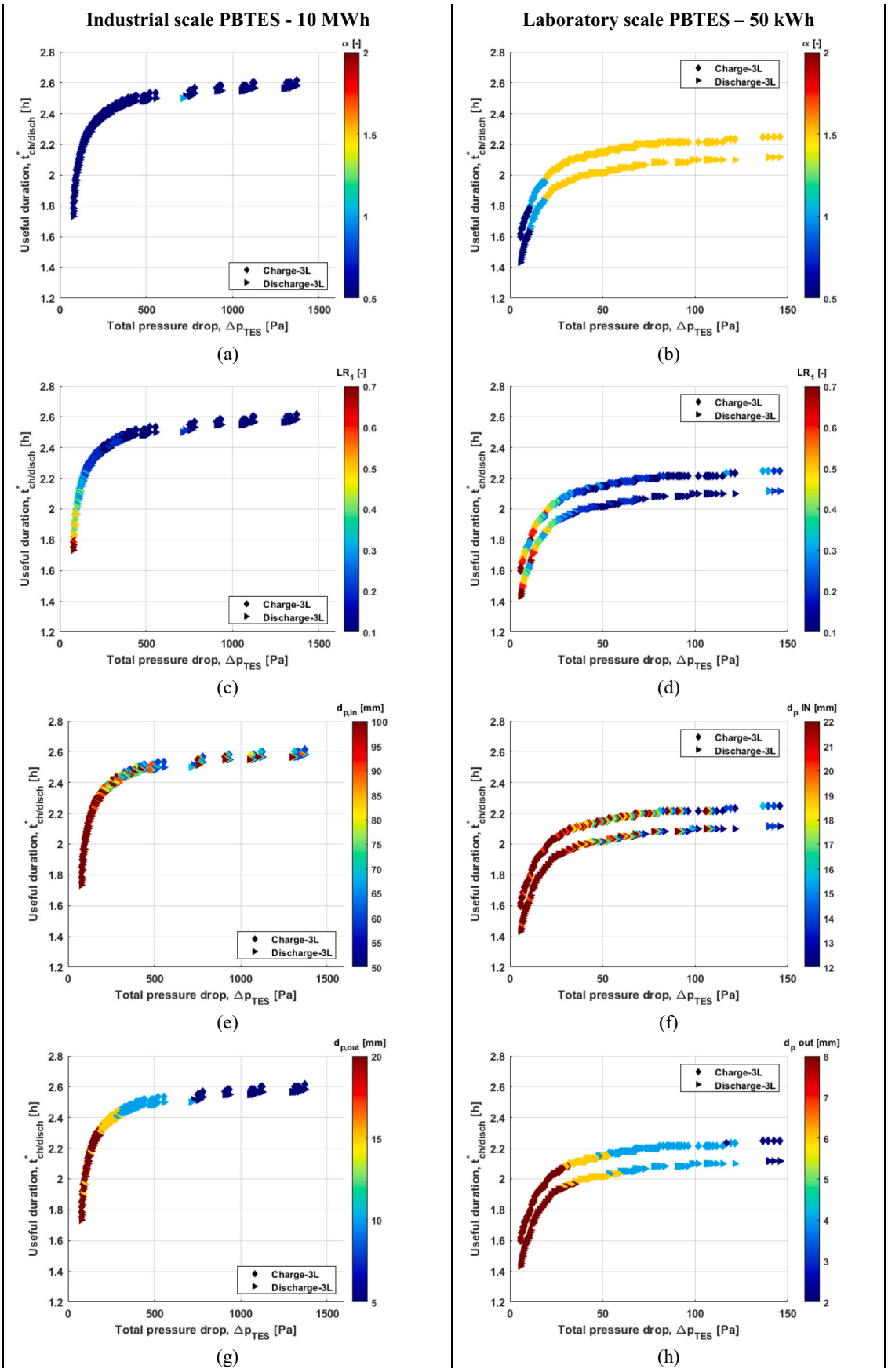

Fig. A. Influence of the aspect ratio (a-b), LR1 (c-d), inner particle size (e-f), and outer particle size (g-h) over the identified Pareto curves for PBTES with 3 coaxial layers and energy capacity of 10 MWh and 50 kWh.

References

[1] IRENA International Renewable Energy Agency, Innovation Outlook: Thermal Energy Storage. Abu Dhabi, 2020.
[2] I. Ortega-Fernández, J. Rodríguez-Aseguinolaza, Thermal energy storage for waste heat recovery in the steelworks: the case study of the REslag project, Appl. Energy 237 (2019) 708–719, https://doi.org/10.1016/j.apenergy.2019.01.007.
[3] J. Michaelis, T. Muller, U. Reiter, F. Fermi, A. Wyrwa, Y.K. Chen, et al., Comparison of the techno-economic characteristics of different flexibility options in the European energy system, Int. Conf. Eur. Energy Mark. EEM (2017) 1–5, https://doi.org/10.1109/EEM.2017.7981983.
[4] IRENA, Global Energy Transformation: A Roadmap to 2050. Abu Dhabi, 2019.
[5] S. Trevisan, R. Guédez, B. Laumert, Thermo-economic optimization of an air driven supercritical CO2 Brayton power cycle for concentrating solar power plant with packed bed thermal energy storage, Sol. Energy 211 (2020) 1373–1391, https://doi.org/10.1016/j.solener.2020.10.069.
[6] T. Esence, A. Bruch, S. Molina, B. Stutz, J.F. Fourmigué, A review on experience feedback and numerical modeling of packed-bed thermal energy storage systems, Sol. Energy (2017), https://doi.org/10.1016/j.solener.2017.03.032.
[7] J. Marti, L. Geissbühler, V. Becattini, A. Haselbacher, A. Steinfeld, Constrained multi-objective optimization of thermocline packed-bed thermal-energy storage, Appl. Energy 216 (2018) 694–708, https://doi.org/10.1016/j.apenergy.2017.12.072.
[8] R. Anderson, S. Shiri, H. Bindra, J.F. Morris, Experimental results and modeling of energy storage and recovery in a packed bed of alumina particles, Appl. Energy (2014) 521–529, https://doi.org/10.1016/j.apenergy.2014.01.030.
[9] Y. Muhammad, P. Saini, K. Knobloch, H.L. Frandsen, K. Engelbrecht, Rock bed thermal energy storage coupled with solar thermal collectors in an industrial application: simulation, experimental and parametric analysis, J. Energy Storage 67 (2023) 107349, https://doi.org/10.1016/j.est.2023.107349.
[10] A. Touzo, R. Olives, G. Dejean, D. Pham Minh, M. El Hafi, J.F. Hoffmann, et al., Experimental and numerical analysis of a packed-bed thermal energy storage system designed to recover high temperature waste heat: an industrial scale up, J. Energy Storage (2020) 32, https://doi.org/10.1016/j.est.2020.101894.
[11] K.G. Allen, T.W. Von Backström, D.G. Kröger, A.F.M. Kisters, Rock bed storage for solar thermal power plants: rock characteristics, suitability, and availability, Sol. Energy Mater. Sol. Cells 126 (2014) 170–183, https://doi.org/10.1016/j.solmat.2014.03.030.
[12] N. Calvet, G. Dejean, X. Py, Waste from Metallurgic Industry: A Suistainable High-Temperature Thermal Energy Storage Material for Concentrated Solar Power, 2013.
[13] A.L. Avila-Marin, M. Alvarez-Lara, J. Fernandez-Reche, A regenerative heat storage system for central receiver technology working with atmospheric air, Energy Procedia (2013), https://doi.org/10.1016/j.egypro.2014.03.076.
[14] M.M.S. Al-azawii, C. Theade, M. Danczyk, E. Johnson, R. Anderson, Experimental study on the cyclic behavior of thermal energy storage in an air-alumina packed bed, J. Energy Storage 18 (2018) 239–249, https://doi.org/10.1016/j.est.2018.05.008.
[15] E.C. Nsofor, Investigations on the packed bed for high-temperature thermal energy storage, Int. J. Green Energy (2005), https://doi.org/10.1080/01971520500287925.
[16] P. Klein, T.H. Roos, T.J. Sheer, Experimental investigation into a packed bed thermal storage solution for solar gas turbine systems, in: Proc. SolarPACES 2013 Int. Conf., 2014, pp. 840–849, https://doi.org/10.1016/j.egypro.2014.03.091.
[17] J.F. Hoffmann, T. Fasquelle, V. Goetz, X. Py, A thermocline thermal energy storage system with filler materials for concentrated solar power plants: experimental data and numerical model sensitivity to different experimental tank scales, Appl. Therm. Eng. (2016), https://doi.org/10.1016/j.applthermaleng.2016.01.110.
[18] C. Odenthal, F. Klasing, P. Knödler, S. Zunft, T. Bauer, Experimental and numerical investigation of a 4 MWh high temperature molten salt thermocline storage system with filler, AIP Conf. Proc. (2020) 2303, https://doi.org/10.1063/5.0028494.
[19] M. Wittmann, M. Schmitz, H.G. Silva, P. Schmidt, G. Doppelbauer, R. Ernst, et al., HPS2 – demonstration of molten-salt in parabolic trough plants – design of plant, AIP Conf. Proc. (2019), https://doi.org/10.1063/1.5117642.
[20] R. Anderson, L. Bates, E. Johnson, J.F. Morris, Packed bed thermal energy storage: a simplified experimentally validated model, J. Energy Storage (2015), https://doi.org/10.1016/j.est.2015.08.007.
[21] E. Johnson, L. Bates, A. Dower, P.C. Bueno, R. Anderson, Thermal energy storage with supercritical carbon dioxide in a packed bed: modeling charge-discharge cycles, J. Supercrit. Fluids 137 (2018) 57–65, https://doi.org/10.1016/j.supflu.2018.03.009.
[22] DLR German Aerospace Center. Test Facility for Thermal Energy Storage in Molten Salt (TESIS:com) n.d. https://www.dlr.de/en/research-and-transfer/research-infrastructure/test-facility-for-thermal-enery-storage-in-molten-salt-tesis-com.
[23] G. Zanganeh, A. Pedretti, S. Zavattoni, M. Barbato, A. Steinfeld, Packed-bed thermal storage for concentrated solar power - pilot-scale demonstration and industrial-scale design, Sol. Energy 86 (2012) 3084–3098, https://doi.org/10.1016/j.solener.2012.07.019.
[24] P. Gauché, South African provisional patent application, in: 2014/03555, 2014.
[25] S. Soprani, F. Marongiu, L. Christensen, O. Alm, K.D. Petersen, T. Ulrich, et al., Design and testing of a horizontal rock bed for high temperature thermal energy storage, Appl. Energy (2019), https://doi.org/10.1016/j.apenergy.2019.113345.
[26] D. Schlipf, E. Faust, G. Schneider, H. Maier, First operational results of a high temperature energy storage with packed bed and integration potential in CSP plants, AIP Conf. Proc. (2017), https://doi.org/10.1063/1.4984445.
[27] S. Trevisan, W. Wang, R. Guedez, B. Laumert, Experimental evaluation of an innovative radial-flow high- temperature packed bed thermal energy storage, Appl. Energy (2022) 311, https://doi.org/10.1016/j.apenergy.2022.118672.
[28] S. Singh, K. Sørensen, T. Condra, S.S. Batz, K. Kristensen, Investigation on transient performance of a large-scale packed-bed thermal energy storage, Appl. Energy 239 (2019) 1114–1129, https://doi.org/10.1016/j.apenergy.2019.01.260.
[29] K. Allen, T. Von Backström, E. Joubert, P. Gauché, Rock bed thermal storage: concepts and costs, AIP Conf. Proc. (2016), https://doi.org/10.1063/1.4949101.
[30] H.F. Laubscher, T.W. Von Backström, F. Dinter, Developing a cost effective rock bed thermal energy storage system: design and modelling, AIP Conf. Proc. (2017), https://doi.org/10.1063/1.4984436.
[31] F. Marongiu, S. Soprani, K. Engelbrecht, Modeling of high temperature thermal energy storage in rock beds – experimental comparison and parametric study, Appl. Therm. Eng. (2019) 163, https://doi.org/10.1016/j.applthermaleng.2019.114355.
[32] E. Faust, D. Schlipf, G. Schneider, H. Maier, Flow modeling of a packed bed high temperature thermal energy storage system, AIP Conf. Proc. 2033 (2018) 1–8, https://doi.org/10.1063/1.5067102.
[33] J. McTigue, A. White, A Comparison of Radial-flow and Axial-flow Packed Beds for Thermal Energy Storage. 8th Int. Conf. Appl. Energy, 2017, pp. 4192–4197, https://doi.org/10.1016/j.egypro.2017.03.893.
[34] R. Daschner, S. Binder, M. Mocker, Pebble bed regenerator and storage system for high temperature use, Appl. Energy 109 (2013) 394–401, https://doi.org/10.1016/j.apenergy.2012.10.062.
[35] S. Trevisan, Renewable Heat on Demand High-Temperature Thermal Energy Storage: A Comprehensive Study From Material Investigation to System Analysis Via Innovative Component Design, KTH Royal Institute of Technology, 2022.
[36] E.W. Lemmon, M.L. Huber, McLinden MO, REFPROP, Reference Fluid Thermodynamic and Transport Properties Database, 2013.
[37] Saint-Gobain NORPRO, Denstone Support Media, 2020.
[38] T.E.W. Schumann, Heat transfer: a liquid flowing through a porous prism, J. Frankl. Inst. (1929), https://doi.org/10.1016/S0016-0032(29)91186-8.
[39] S. Trevisan, Y. Jemmal, R. Guedez, B. Laumert, Packed bed thermal energy storage: a novel design methodology including quasi-dynamic boundary conditions and techno-economic optimization, J. Energy Storage (2021) 36, https://doi.org/10.1016/j.est.2021.102441.
[40] D. Kunii, J.M. Smith, Heat transfer characteristics of porous rocks, AICHE J. 6 (1960) 71–78, https://doi.org/10.1002/aic.690060115.
[41] P. Cheng, C.-T. Hsu, Heat conduction, Transp. Phenom. Porous Media, Pergamon (1998) 57–76, https://doi.org/10.1016/B978-0-08-042843-7.50003-9.
[42] N. Wakao, K. Kato, Effective thermal conductivity of packed beds, J. Chem. Eng. Japan 2 (1969) 24–33, https://doi.org/10.1252/jcej.2.24.
[43] B. Stuke, Berechnung des Wärmeaustausches in Regeneratoren mit zylindrischen und kugelförmigen Füllmaterial, Angew. Chem. 20 (1948) 262–268, https://doi.org/10.1002/ange.19480201004.
[44] B. Xu, P.W. Li, C.L. Chan, Extending the validity of lumped capacitance method for large Biot number in thermal storage application, Sol. Energy 86 (2012) 1709–1724, https://doi.org/10.1016/j.solener.2012.03.016.
[45] S. Ergun, A.A. Orning, Fluid flow through randomly packed columns and fluidized beds, Ind. Eng. Chem. 41 (1949) 1179–1184, https://doi.org/10.1021/ie50474a011.
[46] I. Ortega-Fernández, N. Calvet, A. Gil, J. Rodríguez-Aseguinolaza, A. Faik, B. D'Aguanno, Thermophysical characterization of a by-product from the steel industry to be used as a sustainable and low-cost thermal energy storage material, Energy 89 (2015) 601–609, https://doi.org/10.1016/j.energy.2015.05.153.
[47] I. Calderón-Vásquez, V. Segovia, J.M. Cardemil, R. Barraza, Assessing the use of copper slags as thermal energy storage material for packed-bed systems, Energy (2021) 227, https://doi.org/10.1016/j.energy.2021.120370.
[48] A. Busari, J. Snyman, W. Kupolati, J. Ndambuki, E. Sadiku, R. Loto, et al., Data on the engineering properties of aluminum dross as a filler in asphalt, Data Br 31 (2020) 105934, https://doi.org/10.1016/j.dib.2020.105934.